Starburst amacrine cells amplify optogenetic visual restoration through gap junctions

Yusaku Katada[1,2], Hiromitsu Kunimi[1,2], Naho Serizawa[1,2], Deokho Lee[1,2], Kenta Kobayashi[3], Kazuno Negishi[2], Hideyuki Okano[4], Kenji F. Tanaka[5], Kazuo Tsubota[2], and Toshihide Kurihara[1,2].

[1]Laboratory of Photobiology, [2]Department of Ophthalmology, [4]Department of Physiology, [5]Department of Neuropsychiatry, Keio University School of Medicine, Shinanomachi, Shinjuku-ku, Japan

[3]Section of Viral Vector Development, Center for Genetic Analysis of Behavior, National Institute for Physiological Sciences, National Institutes of Natural Sciences, Okazaki, Aichi, Japan

Corresponding authors:

Toshihide Kurihara, MD/PhD

Laboratory of Photobiology, Department of Ophthalmology, Keio University School of Medicine; 35 Shinanomachi, Shinjuku-ku, Tokyo 160-8582, Japan

Tel.: +81-3-5363-3204, Fax: +81-3- 5363-3274

E-mail: kurihara@z8.keio.jp

Kazuo Tsubota, MD/PhD

Professor and Department Chair, Department of Ophthalmology, Keio University School of Medicine; 35 Shinanomachi, Shinjuku-ku, Tokyo 160-8582, Japan

Tel.: +81-3-5363-3269, Fax: +81-3- 3358-5961

E-mail: tsubota@z3.keio.jp

Abstract

Ectopic induction of optogenetic actuators, such as channelrhodopsin, is a promising approach to restoring vision in the degenerating retina. However, the cell type-specific response of ectopic photoreception has not been well understood. It is limited to obtain efficient gene expression in a specifically targeted cell population by a transgenic approach. In the present study, we established a murine model with high efficiency of gene induction to retinal ganglion cells (RGCs)- and amacrine cells using an improved tetracycline transactivator-operator bipartite system (KENGE-tet system). To investigate the cell type-specific visual restorative effect, we expressed the channelrhodopsin gene into RGCs and amacrine cells using the KENGE-tet system. As a result, enhancement in the visual restorative effect was observed to RGCs and starburst amacrine cells. In conclusion, a photoresponse from amacrine cells may enhance the maintained response of RGCs and further increase/improve the visual restorative effect.

Introduction

Inherited retinal degeneration is one of the major causes of vision loss. More than 2 million people worldwide are blind due to this disease [1], and there is still almost no effective treatment. Previous studies have reported visual restoration effects in animal models by various molecules such as optogenetic actuators [2–9]. In addition, clinical trials have also started using channelrhodopsin 2 (RST-001, ClinicalTrials.gov Identifier: NCT01648452) and Chrimson R (GS-030, ClinicalTrials.gov Identifier: NCT03326336), with gene transduction into retinal ganglion cells (RGCs) by intravitreal injection of recombinant adeno-associated virus (rAAV). Although the visual reconstruction effects by optogenetic gene transfer (such as channelrhodopsin-2 into RGCs[2] and ON-bipolar cells [3,5,6,8,10]) have been shown, interactions between the other types of cells in the retinal neural circuits in optogenetic visual restoration have not been well understood yet. Channelrhodopsin 2 conductance was reported to be 50–250 fS [11], indicating the need for sufficient gene expression to control the membrane potential. In this study, we employed a tetracycline-controllable gene expression system (tet system) [12] in which the amount of gene expression has been much improved (KENGE-tet system) [13]. Furthermore, we established sufficient gene induction in RGCs and amacrine cells. To investigate cell-type-specific visual restorative effects, channelrhodopsin2(E123T/T159C) was ectopically expressed into those

58 cells by KENGE-tet system. As a result, we revealed that amacrine cells may play an
59 essential role in retinal neuronal circuits via gap junctions to enhance the optogenetic visual
60 restorative effect.
61
62 **Results**
63 **Gene induction of RGCs and SACs in M4-YC and RGCs in 5B-YC**
64 We employed two different mouse lines that express the gene encoding the tetracycline
65 transactivation (tTA) protein under the control of a cell-type-specific promoter, muscarinic
66 acetylcholine receptor 4 (*Chrm4*)[14] or 5-hydroxytryptamine (5-HT, serotonin) 5B receptor
67 (*Htr5b*)[13] control region: *Chrm4*-tTA or *Htr5b*-tTA. These mice were further crossed with
68 another transgenic mouse line containing the yellow Cameleon-Nano 50 (YC) fluorescent
69 gene connected into the downstream of the tet operator (tetO) promoter [15]. The YC gene
70 expression was induced only by the presence of tTA protein in the double transgenic mice
71 (*Chrm4*-tTA::tetO-YC (M4-YC) or *Htr5b* -tTA::tetO-YC (5B-YC)) (Figure S1A, B). The
72 expression of YC was observed in the double transgenic mouse retina with a fluorescence
73 microscope. In the M4-YC mouse retina, we identified the expression of YC in RGCs
74 (Figure 1A-D, Figure S2A-E) and amacrine cells (Figure 1A-D, Figure S1E-F) with *in vivo*
75 fluorescence microscopy and in sections. In the 5B-YC mouse retina, we identified the
76 expression of YC in RGCs (Figure 1E-H) and the corneal stromal layer (Figure S2G-M)

77 with *in vivo* fluorescence microscopy and in sections. In both lines, no expression was found
78 in displaced amacrine cells, only RGCs were labeled in the ganglion cell layer, and the
79 percentage of YC-positive cells in RGC marker RBPMS [16]-positive cells was 35.4% (n=5)
80 in M4-YC and 36.5% (n=5) in 5B-YC from RGCs, which were equivalent (Figure 1I-L, O-
81 R, Figure S2M-Q). All of the amacrine cell expression in the M4 line was choline
82 acetyltransferase (ChAT) staining-positive and consisted of starburst amacrine cells (SACs),
83 and 31.1±2.1 % (n=3) of ChAT-positive cells were YC-positive (Figure 1M-T, Figure S3
84 A-L).
85
86 As a visual restoration model, the *Chrm4*-tTA and *Htr5b*-tTA line were crossed with tetO-
87 channelrhodopsin2(E123T/T159C) (tetO-ChR2) mice [17] (Figure S1C). *Chrm4*-tTA::tetO-
88 ChR2 (M4-ChR2) drove ChR2 expression in both RGCs and amacrine cells and *Htr5b* -
89 tTA::tetO-ChR2 (5B-ChR2) only in RGCs in the retina. In the retinas of these double
90 transgenic mice, photoreceptor degeneration was induced by intraperitoneal injection of N-
91 methyl-N-nitrosourea (MNU) [18]. MNU is an alkylating agent that causes DNA methylation
92 in the O6 position of guanine, resulting in apoptosis, and it has been widely used to induce
93 a pharmacological animal model of retinitis pigmentosa (RP). Two weeks after 75 mg/kg
94 MNU administration into the mice at the age of 8 weeks, the outer nuclear layer containing

95 photoreceptors was largely absent (Figure S4A, B), and the light-evoked response from
96 photoreceptors was not detected by electroretinography (ERG) (Figure S4C).
97 TUNEL assay was performed to determine whether there was any neurotoxicity-induced
98 cell death in the retina due to Channel rhodopsin expression, however, we could not observe
99 any cell death in the retina (Figure S4D).
100
101 **M4-ChR2 mouse shows higher visual restorative effect.**
102 To evaluate the function of the channelrhodopsin ectopically induced in the transgenic
103 mouse retinas, we performed multi-electrode array (MEA) recording, which can record
104 extracellular potentials of RGCs (Figure S4E). As a result of photoreceptor degeneration
105 induced with MNU treatment, the control retina without channel-rhodopsin expression
106 (tetO-ChR2) showed no response from RGCs detected (Figure 2A). In contrast, the M4-
107 ChR2 (Figure 2B) and 5B-ChR2 (Figure 2C) retinas showed obvious light-induced
108 responses. After filtering with the Gaussian function (Figure 2D, E), the maintained
109 response after the peak was significantly greater in M4-ChR2 mice than in 5B-ChR2 mice
110 (Figure 2F), which indicates that the light-evoked ON response in RGCs could be modified
111 through the response from amacrine cells.
112

113 To investigate whether light reception on the retina is transmitted to the visual cortex, we
114 then examined visual evoked potentials (VEPs) from the visual cortex (Figure 2G). The
115 output from RGCs is sent through the axons of RGCs (the optic nerve) to the lateral
116 geniculate nucleus (LGN) of the thalamus, which is a region of the mesencephalon, from
117 the LGN to the primary visual cortex (V1) in the occipital lobe of the cerebral cortex. VEPs
118 were not detected in the control tetO-ChR2 mice with MNU treatment (Figure 2H, I). In
119 contrast, VEPs were observed in both M4-ChR2 and 5B-ChR2 mice treated with MNU
120 (Figure 2H, I). In response to the light stimulus at 4000 cds/m^2, the average of the VEP
121 amplitude in MNU-treated M4-ChR2 mice was significantly higher (143.6 μV; n=12,
122 P=0.03) than in MNU-treated 5B-ChR2 (79.6 mV; n = 12) and the same level as in the mice
123 without MNU treatment (155 μV; n=4). However, the shapes of the waveforms were
124 irregular in both models compared to controls, and their physiological roles are unknown.
125 Thus, there is a limitation in this direct comparison.
126
127 To validate the model system, we also examined the MEA, ERG and VEPs of M4-ChR2
128 and 5B-ChR2 in the absence of retinal degeneration (no MNU treatment and no mutation).
129 As a result of MEAs, the peak response was significantly reduced in both lines and further
130 reduced with MNU treatment (Figure S4F). A similar trend was observed for the maintained

131 response, whereas it was maintained in the M4 line (Figure S4G). This finding suggests that
132 channelrhodopsin gene induction into healthy RGCs interferes with the physiological retinal
133 light response. In addition, in the control mice, not only the ON response but also the OFF
134 response was confirmed. In contrast, the OFF response was significantly lost in the M4 line
135 (Figure S4I). It is known that SACs in the INL are connected to off bipolar cells [19], which
136 might be related to this change. As a result of ERG and VEPs, both lines tended to have
137 shorter latencies, especially in photopic examinations (Figure S5E, I, L, O), likely because
138 of the channelrhodopsin response to strong light [9] and its photoreception in RGCs resulting
139 in short latency [2]. Although the amplitude of both ERG and VEP tended to be small in the
140 5B line (Figure S5C, G, M, N), these measurements were not significant, and there was no
141 significant change in the shape of the waveforms.
142
143 Next, light-dark transition testing (LDT) was performed to investigate whether ectopic
144 expression of channelrhodopsin in the degenerative retinas may lead to behavioral changes
145 according to visual restoration. Rodents tend to stay in dark places according to their visual
146 function since they are nocturnal and feel uneasy in bright environments (Figure 2J), while
147 the visually disturbing MNU-treatment (Figure 2K) resulted in almost half of the staying
148 time in bright and dark places (ratio in bright half at 10 min was closer to 0.5). In contrast,

149 both the M4-ChR2 and 5B-ChR2 mouse lines with each MNU-treatment showed decreased
150 staying time in bright places, indicating that visual restoration was confirmed in these
151 models. Furthermore, M4-ChR2 mice showed significantly higher visual restorative effects
152 than 5B-ChR2 mice (Figure 2K).

153 We also examined the optokinetic response (OKR) to investigate whether light receptivity
154 in the retina restored by ectopic channelrhodopsin expression could lead to central reflex
155 movement output. In OKR, a rotating striped pattern was displayed to the head-fixed mice
156 to induce eye movements, and the velocity was measured to evaluate the integrity of the
157 subcortical reflex circuitry of the mice (Figure S6A). OKR was not detected in the mice
158 with MNU administration except for the M4 line (4.80 deg/sec, n=6) (Figure S6B).

159 This outcome seems to be due to lack of ChR2 expression in SACs, which play a key role
160 in OKR [20], in the retinas of 5B-ChR2 mice. We also examined *rd1* mice as a genetic animal
161 model of RP. These mice have a nonsense mutation in the *Pde6b* gene leading to rapid
162 degeneration of rods, photoreceptors followed by loss of cones [21,22]. We used blind *rd1*
163 mutation mice at the age of 10-12 weeks for the following experiments. In the cases of *rd1*
164 mutant mice, no detectable OKR was observed in any combinations with each transgenic
165 line, including M4-ChR2. To investigate the dissociation of OKR between the MNU-
166 treatment and *rd1* models, the retinal thickness was compared under the same conditions

167 above. As a result, the total retinal thickness of *rd1* mice (78.3 μm; n=9) was significantly
168 thinner than that of MNU-treated mice (97.2 μm; n=10) evaluated on optical coherence
169 tomography (OCT) (Figure S6C, D). This outcome was thought to be because the inner
170 retinal layer was thinner of the *rd1* mouse (Figure S6E). Indeed, the inner nuclear layer of
171 the *rd1*, *rd1*;5B-ChR2 and *rd1*;M4-ChR2 mice was significantly thinner than that of the
172 MNU-treated mice (Figure S6F) and YC-positive cells in the inner retinal layer of *rd1*;M4-
173 ChR2 tended to be fewer than those in the inner retinal layer of MNU-treated mice (Figure
174 S6G), suggesting that SACs in the inner layer may be degenerated. This result suggests that
175 residual inner retinal thickness and its durability might be potential limitations of
176 optogenetic gene therapy in inherited retinal disease patients clinically.
177

178 **Acetylcholine and gap junctions are involved in the maintained response**

179 The M4-ChR2 mouse line, which showed the transgene expression in amacrine cells in
180 addition to RGCs, showed a higher maintained response and more effective visual
181 restoration (Figure 2) than the 5B-ChR2 mice. Therefore, we investigated the neurocircuit
182 pathway responsible for the enhanced response due to amacrine cells using neurotransmitter
183 blockers on the MEA recording. Administration L-2-amino-4-phosphonobutyric acid (L-
184 AP4), which is an agonist for group III metabotropic glutamate receptors, including

185 mGluR6 working as a blocker of retinal ON-bipolar cells, did not show significant changes
186 in either MNU-treated M4-ChR2 (Figure 3A-C) or 5B-ChR2 (Figure 3D-F) retinas, which
187 indicates that the photoresponse was not derived from photoreceptors. In contrast,
188 administration of mefenamic acid (MFA) or carbenoxolone, an inhibitor of gap junctions,
189 induced a significant decrease in the maintained response but not the peak of the response
190 in the MNU-treated M4-ChR2 retina (Figure 3G-I, Figure S7A-C). This change was
191 recovered after washout and not observed in the 5B-ChR2 retina (Figure S7D-F). SACs
192 release GABA and acetylcholine [23]. Thus, we also examined inhibitors of GABA receptors,
193 bicuculline for GABA-A, CGP 52432 for GABA-B and (1,2,5,6-tetrahydropyridin-4-yl)
194 methylphosphinic acid (TPMPA) for GABA-C receptors, and cholinergic antagonists,
195 mecamylamine for nicotinic and atropine for muscarinic acetylcholine receptors. As a result,
196 no significant change was observed with the administration of GABA receptor blockers
197 (Figure S7G-O) and mecamylamine (Figure S7P-R), but atropine administration showed a
198 similar decrease in maintained response and peak response in the MNU-treated M4-ChR2
199 mice (Figure 3J-L). In addition, to determine whether this change may occur via bipolar
200 cells, an AMPA receptor antagonist, 6-cyano-7-nitro-quinoxaline-2,3-dione (CNQX), and
201 an NMDA receptor antagonist, D(-)-2-amino-5-phosphonopentanoic acid (D-AP5), were
202 administered. As a result, no statistically significant difference was observed, although there

203 was a tendency toward a decrease in the maintained response (Figure S7S-U). SACs form
204 synapses with bipolar cells, RGCs, and other amacrine cells [23–25]. It is also known that
205 amacrine cells are directly connected with RGCs through gap junctions [26,27], regulating
206 neural circuits in the retina [28]. Therefore, these results indicated that SACs enhanced the
207 maintained response of RGCs directly or indirectly through muscarinic acetylcholine and
208 gap junctions.
209
210 MEA showed a visual restoration effect induced by ectopic ChR2 expression in the
211 degenerative retina (Figure 2). These photoresponses obtained from MEA were all ON
212 responses, as previously reported [2,29,30,31.] Several slow photoresponses obtained from RGCs
213 were considered to have an ipRGC origin [32], and they were excluded from the data. The
214 MNU-treated M4-ChR2 retina showed a significant more enormous response in the
215 maintained time phase compared to 5B-ChR2. As a result of a neurotransmitter blocking
216 test (Figure 4), inhibition of muscarinic acetylcholine and gap junctions decreased the
217 sustained response of only M4-ChR2 retinas. The difference between M4-ChR2 and 5B-
218 ChR2 was the presence or absence of ChR2 gene expression in SACs. Therefore, it was
219 suggested that photoresponse from SACs enhanced the maintained response of RGCs,
220 enhancing the visual restoration effect via muscarinic acetylcholine and gap junctions.
221

222 **Induction efficiency into SACs tends to affect visual restoration.**

223 Finally, to investigate its clinical applicability, the effect of SACs on visual restoration was
224 examined using rAAV2 which was approved for gene therapy [33]. We injected rAAV2-CAG-
225 ChR2-tdimer2 intravitreally into *rd1* mice and performed MEA, VEPs, and LDT (Figure
226 4A, Figure S8A, B). In addition, we counted the number of transfected RGCs and SACs and
227 analyzed their relevance to visual restorative effects. As a result of immunohistochemical
228 labeling using RBPMS, the infection efficiency to RGCs was 24%, which was equivalent
229 to previous reports (21-23%) [2,34,35], and significantly less than those of our transgenic mice
230 (Figure 4B, C). The efficiency of SACs was 12%, which was also less than that of transgenic
231 mice (Figure 4D, E). As a result of MEA recording, the peak response in the rAAV model
232 was equivalent to that of both transgenic lines (Figure S8C). The maintained response and
233 its rate were equal to that of the M4 line (Figure S8D, E), perhaps because the input from
234 various cell types other than SACs is also included in the rAAV model. The increased
235 maintained response may be affected by gene transfer to cells other than SACs, but similar
236 characteristics to the M4 line have been obtained. Each average of the VEP amplitude in
237 the *rd1*;M4-ChR2, *rd1*;5B-ChR2, and rAAV-treated *rd1* mice in response to the light
238 stimulus at 4000 cds/m^2 was 72.7 μV (n=10), 70.4 μV (n=12) and 32.2 μV (n=12),
239 respectively. These responses were significantly higher than those in *rd1*;tetO-ChR2 mice

240 (19.1 mV; n=8) but smaller than those in the 8-week-old wild-type C57BL/6J mice (155 μV;
241 n=4) (Figure 4F, G). There was no significant difference between *rd1*;5B-ChR2 and *rd1*;
242 M4-ChR2 mice, and the VEPs of rAAV treated *rd1* mice were smaller than those of them
243 (Figure 4F, G). Even in the LDT results, the restorative effect of rAAV-treated *rd1* mice
244 tended to be lower than that of transgenic mice (Figure 4H), perhaps due to its infection
245 efficiency or the higher maintained response might not lead directly and simply to better
246 visual restoration. In addition, the correlation between the infection efficiency of SACs in
247 each rAAV-treated *rd1* mouse and the visual restorative effect was investigated. The results
248 showed a significant, positive correlation between the number of transfected SACs in the
249 inner nuclear layer and the maintained to peak ratio in MEA (Figure 4I), a positive
250 correlation between the VEP amplitudes (Figure 4J), and a significant, negative correlation
251 between the time spent in the bright half in LDT (Figure 4K). This outcome suggests that
252 the maintained response in MEA is derived from SACs and that, clinically, the inclusion of
253 SACs, rather than only RGCs, which is the primary target of optogenetic therapy, is effective
254 for visual restoration. Although there is a limitation because infection efficiency is a
255 confounding factor, there was no correlation between the number of transfected RGCs in
256 the ganglion cell layer and the maintained to peak ratio in MEA (Figure S8F). The
257 correlation of the number of transfected SACs in the inner nuclear layer with the VEP

258 amplitudes (Figure 4J) and the time spent in the bright half in LDT (Figure 4K) was stronger
259 than that with infection efficiency into RGCs (Figure S8G, H).
260

261 **Discussion**

262 In this study, we established transgenic mouse lines inducing gene induction in specific
263 retinal cells using the tet-system (Figure S1). We identified that gene induction occurred in
264 RGCs and SACs under the control of a muscarinic acetylcholine receptor *Chrm4* promoter.
265 In contrast, serotonin (5-HT) *Htr5b* receptor control region led to induction only in RGCs
266 in the retina (Figure 2). Among acetylcholine receptors expressed by all types of neurons in
267 the retina [36–41], the *Chrm4* muscarinic receptor is expressed in RGCs and amacrine cells [36,42].
268 All of the amacrine cell expressions in the M4 line consisted of type-a SACs (Figure 1M-T,
269 Figure S3 A-L). There are two subtypessubtypes of SACs, type-a, and type-b (displaced
270 SACs)[43,44]. This would be the first report of a transgenic line specific to only type-a but not
271 type-b SACs. Approximately 30% of the type-b SACs were expressed in the M4 line, and
272 no noticeable morphological differences were observed between positive and negative
273 SACs. The 5-HT *Htr5b* receptor is expressed in rodents but not in humans [45]. Although
274 several types of 5-HT receptors are expressed in the mouse retina [46], the retinal distribution
275 of the *Htr5b* receptor has not been previously described to our knowledge. We found that

276 these gene inductions in both mouse retinas are useful for examining the functions of RGCs
277 and SACs.
278
279 Accumulating data have shown that the visual restoration strategy induced by optogenetic
280 genes is a promising therapy for degenerative retinal diseases. Most amacrine cells are
281 inhibitory neurons in the vertebrate retina, which have not been regarded much in the
282 elementary visual restoration target. This study showed that SACs increased the
283 maintained response through gap junctions and contributed to enhancing the visual
284 restorative effect. In particular, since the restorative effect of LDT and OKR was more
285 significant than that of VEPs, it might contribute to sustained behavior and direction
286 recognition rather than transient response, consistent with the role of the maintained
287 response in RGCs [47]. Including the results using rAAV, in the current situation, viral
288 delivery in primates is limited [29], and gene transfer involving amacrine cells, for example,
289 using ubiquitous promoters, might be more effective in visual restoration than limiting
290 RGCs in the clinical setting.
291

292 In conclusion, this study suggests that the optogenetic photoresponse from SACs

293 enhances the maintained response, which further enhances the visual restoring effect.

294 These results may provide the basis for advanced visual restoration in the future.

295

296 **Methods**

297 **Key Resources Table**

REAGENT or RESOURCE	SOURCE	IDENTIFIER
Chemicals, Peptides, and Recombinant Proteins		
N-Nitroso-N-methylurea	Toronto Research Chemicals	M325815
Domitor® (medetomidine hydrochloride)	Zenoac	
Antisedan® (atipamezole)	Zenoac	
Midazolam Sandoz™	Sandoz	
Vetorphal® (butorphanol)	Meiji Seika Pharma	
Ames' Medium	Sigma	A1420
L-AP4	Abcam	ab120002
Meclofenamic acid sodium salt	Sigma	M4531
TPMPA	TOCRIS	1040
Bicuculline	Wako	026-16131
CGP 52432 hydrochloride	Sigma	SML0593
Mecamylamine	TOCRIS	2843/10
CNQX	Abcam	ab120044
D-AP5	Abcam	ab120003
Carbenoxolone	MERCK	C4790
Atropine	MERCK	A0132
DAPI	Life Technologies	D21490
Anti-RBPMS antibody	Abcam	ab194213
Anti-Choline Acetyltransferase Antibody	Abcam	ab114p
Anti-VGluT2	Frontier Institute	VGluT2-Rb-Af720

Anti-Syntaxin antibody	Abcam	ab3265
Anti-Tyrosine Hydroxylase antibody	Abcam	ab112
Anti-Prox1 antibody	AngioBio	11-002P
pAAV CAG ChR2 E123T T159C 2A tDimer	Addgene	#85399
Experimental Models: Organisms/Strains		
Mouse: C3H/HeJJcl	CLEA Japan	
Mouse: tetO-YCnano50	RIKEN BRC	RBRC09550
Mouse: tetO-ChR2 (E123T/T159C)	RIKEN BRC	RBRC05843
Mouse: *Chrm4*-tTA	RIKEN BRC	RBRC09551
Mouse: *Htr5b*-tTA	RIKEN BRC	RBRC05445
Oligonucleotides		
Genotyping primer: tet-Foward: CATGAAGCAGCACGACTTCTT		
Genotyping primer: tet-Reverse: TTCTTACTTGTACAGCTCGTCCA		
Genotyping primer: M4-Foward: AAGCACCAAGTTCTCTCCCGTCTT		
Genotyping primer: M4-Reverse: CGGAGTTGATCACCTTGGACTTGT		
Genotyping primer: 5B-Foward: GCTCCAGGAAACCACAATGCCTTT		
Genotyping primer: 5B-Reverse: CGGAGTTGATCACCTTGGACTTGT		
Genotyping primer: *rd1*-Forward: AAGCTAGCTGCAGTAACGCCATTT		
Genotyping primer: wild-Forward: ACCTGCATGTGAACCCAGTATTCTATC		
Genotyping primer: *rd1* wild common-Reverse: CTACAGCCCCTCTCCAAGGTTTATAG		

298

299 **Animals**

300 Transgenic mice used for the experiments and their genotyping protocols were generated as
301 previously reported[13]. Mice homozygous for the retinal degeneration alleles Pde6b^{rdl}
302 (C3H/HeJJcl, *rd1*) and WT C57BL/6J were obtained from CLEA Japan, Inc. Animals were
303 maintained under 12-h light:12-h-dark conditions. For animals bred in-house, littermates of
304 the same sex were randomized to experimental groups. Mice used for the experiments were
305 heterozygous for the tTA and tetO genes and homozygous for the *rd1* gene. All of the animal
306 experiments were conducted under protocols approved by the Institutional Animal Care and
307 Use Committee of Keio University School of Medicine.
308 tetO-YC (RBRC09550), tetO-ChR2 (RBRC05843), *Chrm4*-tTA (RBRC09551), and *Htr5b*-
309 tTA (RBRC05445) are available from RIKEN Bioresource Center in Japan.
310 Study approval: All of the animal experiments were conducted under protocols approved by
311 the Institutional Animal Care and Use Committee of Keio University School of Medicine
312 (#2808).
313
314 **Immunohistochemistry**
315 The protocol for immunohistochemistry as previously described[48]. The retinas were
316 incubated in phosphate-buffered saline (PBS) with 1% Triton X-100 and 0.5% Tween 20
317 for 1 h at room temperature and in 4% BSA for 1 h at room temperature and then incubated

318 overnight at 4 ˚C with primary antibodies: RBPMS (1:500, Abcam, Cambridge, UK), ChAT
319 (1:100, Abcam), VGLUT2 (1:100, Frontier Institute, Hokkaido, Japan), syntaxin (1:100,
320 Abcam), tyrosine hydroxylase (1:100, Abcam) and Prox1 (1:100, AngioBio, San Diego, CA,
321 USA) in blocking buffer. Secondary anti-rabbit, mouse, and goat IgG, conjugated with
322 Alexa TM488, TM594, and 633, respectively (1:1000; Molecular Probes), were applied for
323 1 h at room temperature. The retinas then were flat-mounted, and the sections were mounted
324 on slide glass. The TUNEL assay was performed based on our previous reports[49,50].
325

326 **Vector production and purification**

327 pAAV-CAG–ChR2(E123T/T159C)-tdimer2–WPRE (Addgene, Watertown, MA) was used
328 for the current study. Type 2 serotypes of rAAV vectors were prepared using the AAV Helper
329 Free Packaging System (Cell Biolabs, San Diego, CA, USA). The serotypes were produced
330 in HEK293 cells using a helper virus-free system and were purified using two $CsCl_2$ density
331 gradients and titrated by quantitative polymerase chain reaction. Final preparations were
332 dialyzed against PBS and stored at -80°C.
333

334 **Virus injection**

335 The mice were anesthetized with a combination of midazolam, medetomidine, and
336 butorphanol tartrate at doses of 4 mg/kg, 0.75 mg/kg, and 5 mg/kg of body weight and
337 placed on a heating pad that maintained their body temperatures at 35–36°C throughout the
338 experiments. An aperture was made subsequent to the limbus through the sclera with a 30-
339 gauge disposable needle, and a 33-gauge unbeveled blunt-tip needle on a Hamilton syringe
340 was introduced through the scleral opening into the vitreous space for intravitreal injections
341 and introduced through the scleral opening along the scleral interior wall into the subretinal
342 space for subretinal injections. Each eye received 1 μl of vehicle (PBS) or vector at a titer
343 of 2.0×10^{11} vg/ml.
344

345 **Multielectrode array recordings (MEA)**

346 All of the MEA procedures were performed under dim red light. The mice were anesthetized
347 and euthanized by quick cervical dislocation. Following enucleation, the retina was
348 dissected at room temperature in Ames' medium bubbled with 95% O2/5% CO2 (A 1420;
349 Sigma-Aldrich). The separated retina was placed on a cellulose membrane, and RGCs were
350 directed to the electrode and was gently contacted against MEA (MEA2100-Systems; Multi-
351 Channel Systems, Reutlingen, Germany) under suction pressure. During the experiment,
352 the retinas were continuously perfused with Ames' medium bubbling at 34 ° C. at a rate of

353 1-2 ml/min. Recorded signals were collected, amplified, and digitized using MC Rack
354 software (Multi-Channel Systems). Retinas were perfused for 30 min in darkness before
355 recording responses. A 470-nm blue LED light was used at 1.0×10^{16} photons· cm−2· s−
356 1 stimulus. L-(+)-2-amino-4-phosphonobutyric acid (L-AP4, ab120002; Abcam), (1,2,5,6-
357 tetrahydropyridin-4-yl) methylphosphinic acid (TPMPA, Cat. No. 1040; Tocris Bio-
358 Science), meclofenamic acid sodium salt (MFA, M4531; Sigma-Aldrich), atropine (A0132;
359 MERCK), carbenoxolone (C4790; MERCK), Bicuculline (026-16131; Wako), CGP52432
360 (SML0593; Sigma) and Mecamylamine (2843/10, TOCRIS) were newly diluted to 20 μM,
361 20 μM, 100 μM, 20 μM, 100 μM, 10μM, 20 μM and 20 μM respectively. Stimulation was
362 presented for 1 second at 60-second intervals. Signals were filtered between 200 Hz (low
363 cutoff) and 20 kHz (high cutoff). A threshold of 40 μV was used to detect action potentials,
364 and action potentials from individual neurons were determined via a standard expectation–
365 maximization algorithm using Off-line Sorter software (Plexon, Dallas, TX, USA). The
366 results were plotted using NeuroExplorer software (Nex Technologies Colorado Springs,
367 CO, USA). Maintained-to-peak amplitude ratio was calculated by dividing the maintained
368 response amplitude in maintaining time frame (0.4 to 1.0 seconds after light stimulation) by
369 the peak amplitude (this ratio quantifies the sustenance of the response).
370

371 **ERG analyses**

372 Scotopic ERG was recorded according to our previous report [48]. Animals were dark-adapted
373 for 12 h and prepared under dim red illumination. The pupils were dilated with a mixed
374 solution of 0.5% tropicamide and 0.5% phenylephrine (Mydrin-P; Santen, Osaka, Japan).
375 Then, the mice were anesthetized with a combination of midazolam, medetomidine, and
376 butorphanol tartrate at doses of 4 mg/kg, 0.75 mg/kg, and 5 mg/kg of body weight,
377 respectively, and were placed on a heating pad that maintained their body temperature at
378 35–36°C throughout the experiments. The ground electrode was a subcutaneous needle in
379 the tail, and the reference electrode was placed subcutaneously between the eyes. The active
380 contact lens electrodes (Mayo, Inazawa, Japan) were placed on the corneas. Recordings
381 were performed with a PuREC acquisition system (Mayo). Responses were filtered through
382 a bandpass filter ranging from 0.3 to 500 Hz to yield a- and b-waves. White LED light
383 stimulations of 10.0 log cd-s/m^2 were delivered via a Hemisphere LS-100 Stimulator
384 (Mayo).

385

386 **VEP analyses**

387 The measuring electrodes for VEP analyses were placed more than one week before the
388 measurement. The mice were anesthetized with a combination of midazolam, medetomidine,

389 and butorphanol tartrate at doses of 4 mg/kg, 0.75 mg/kg, and 5 mg/kg of body weight,
390 respectively. The animals were placed in a stereotaxic holder. A stainless-steel screw
391 (M1.0×6.0 mm) inserted through the skull into both visual cortex (1.5 mm laterally to the
392 midline, 1.5 mm anterior to the lambda), penetrating the cortex to approximately 1 mm,
393 served as a measuring electrode.
394 At the measurement time, the mice were anesthetized again with the same doses. Visual
395 stimuli were generated by a white LED placed 3 cm from the eye. It was stimulated with
396 100-ms pulses of white LED 4000 cds/m^2 light stimulus intensity. Signals were acquired
397 and analyzed with a PuREC acquisition system (Mayo). Signals were low-pass filtered at
398 300 Hz and averaged over the 60 trials.
399
400 **OKR recording system**
401 Protocols for eye movement recording and visual stimulation were previously described [51,52].
402 Eye movements were recorded from both eyes of each animal separately. During the
403 recording, the contralateral eye was covered by aluminum foil. The head of the mouse was
404 fixed to an experimental steel board by the head-mounted stick for the LIM lens frames.
405 The reflected images through a hot mirror (43957-J, Edmund) were recorded using an
406 infrared CCD camera (BS-GV200, Libraly Inc., Tokyo, Japan). The images of the eye

407 movements were processed and analyzed using software (Move-tr/2D, Libraly Inc., Tokyo,
408 Japan). The sampling rate of the image was 200 Hz. The center of the pupil was detected by
409 the software. We calculated the speed of the eye movements on two-dimensional images
410 and converted them to angular speeds using the AL of each eye. The spatial frequency was
411 set as 0.125 cycles/degree, and the temporal frequency of the visual stimulus was 1.5 Hz.
412 The motion onset delay (MOD) was set as 333 msec. Continuing the MOD, sinusoidal
413 grating started to move clockwise in 5 sec. The intervals of the visual stimulus were 60 sec.
414 Eye movements were recorded three times for each experiment to exclude shaking images
415 due to excessive body movements. Average velocities of the eye movements were calculated
416 in the slow speed phase of their nystagmus.
417
418 **LDT recording**
419 Mice were tested in a 30 × 45 × 30-cm box containing equally sized light and dark chambers
420 connected by a 5 × 5-cm opening via which mice could move freely. The bright half of the
421 box was illuminated from above by a white fluorescent light with an intensity of 200 lux
422 measured at the floor level. The animals were placed in the bright half, and movement was
423 recorded (HD Pro Webcam C920, Logitech, Lausanne, Switzerland). A trial lasted 10 min,
424 and then the testing apparatus was dismantled and cleaned with 70% ethanol. Videos were

425 analyzed using ANY-maze tracking software and were validated by comparison with
426 manual analysis. Time spent in the bright half was recorded.
427
428 **Preparation of whole-mount samples and cryosections of retinas**
429 Enucleated eyes were fixed for 20 min in 4% paraformaldehyde (PFA) in PBS and then
430 dissected as previously described [53]. The obtained tissues were post-fixed overnight in 4%
431 PFA and stored in methanol at –20°C. Cryosections of retinas (12 mm) were prepared as
432 previously described [54] after the eyeballs were immersed overnight in 4% PFA. Retinal
433 sections were observed using a confocal microscope (LSM710; Carl Zeiss, Jena, Germany).
434
435 **OCT Imaging**
436 The thickness of the retina was analyzed by an SD-OCT system (Envisu R4310; Leica,
437 Wetzlar, Germany) tuned for mice. The imaging protocol entailed a 3 mm×3 mm perimeter
438 square scan sequence producing a single en-face image of the retina through a 50-degrees
439 field of view from the mouse lens, following mydriasis. The en-face image consisted of 100
440 B-scan tomograms, with each B-scan consisting of 1000 A-scans. The retinal thickness of
441 150 μm from the optic disc of each quadrant was measured.
442

443 **Quantification and Statistical Analysis**

444 All of the results are expressed as the mean ± SEM. The averaged variables were compared

445 using the Student's 2-tailed t-test and the Kruskal Wallis one-way ANOVA test. P-values of

446 less than 0.05 were considered statistically significant.

447

448 **Data and Software Availability**

449 Raw MEA spike data were sorted offline to identify single units using Offline Sorter

450 software (version 4.4.0)(Plexon). Spike-sorted data were analyzed with NeuroExplorer 5

451 software (version 5.115) (Nex Technologies).

452

Author Contribution

Y.K. and T.K. designed the research, wrote the manuscript, and performed the retinal histology, MEA, ERG and VEP recordings, and LDT experiments. K.K. performed AAV production. Y.K. and H.K. performed OKR recordings. N.S. performed MEA. D.L. performed a TUNEL study. Y.K. performed data processing and analysis. K.N., H.O, and T.K. made critical revisions to the manuscript. T.K. supervised the research.

Acknowledgments

We would like to thank Prof. Amane Koizumi for critical comments to the manuscript. Y.K. is supported by grants from the Keio University Doctorate Student Grant-in-Aid Program. T.K. is supported by Grants-in-Aid from Takeda Science Foundation and the Keio University Medical Science Fund.

Declaration of Interests

The authors declare no competing interests.

469 **References**

470 1. Sahel, J.-A., Marazova, K. & Audo, I. Clinical characteristics and current
471 therapies for inherited retinal degenerations. *Cold Spring Harb. Perspect. Med.* **5**,
472 a017111 (2014).

473 2. Bi, A. *et al.* Ectopic Expression of a Microbial-Type Rhodopsin Restores Visual
474 Responses in Mice with Photoreceptor Degeneration. *Neuron* **50**, 23–33 (2006).

475 3. Doroudchi, M. M. *et al.* Virally delivered Channelrhodopsin-2 Safely and
476 Effectively Restores Visual Function in Multiple Mouse Models of Blindness.
477 *Mol. Ther.* **19**, 1220–1229 (2011).

478 4. Lagali, P. S. *et al.* Light-activated channels targeted to ON bipolar cells restore
479 visual function in retinal degeneration. *Nat. Neurosci.* **11**, 667–675 (2008).

480 5. Cronin, T. *et al.* Efficient transduction and optogenetic stimulation of retinal
481 bipolar cells by a synthetic adeno-associated virus capsid and promoter. *EMBO*
482 *Mol. Med.* **6**, 1–16 (2014).

483 6. Macé, E. *et al.* Targeting channelrhodopsin-2 to ON-bipolar cells with vitreally
484 administered AAV restores ON and OFF visual responses in blind mice. *Mol.*
485 *Ther.* **23**, 7–16 (2014).

486 7. Busskamp, V. *et al.* Genetic Reactivation of Cone Photoreceptors Restores

487 Visual Responses in Retinitis Pigmentosa. *Science (80-.).* **329**, 413–417 (2010).

488 8. Van Wyk, M., Pielecka-Fortuna, J., Löwel, S. & Kleinlogel, S. Restoring the ON
489 Switch in Blind Retinas: Opto-mGluR6, a Next-Generation, Cell- Tailored
490 Optogenetic Tool. *PLoS Biol* **13**, (2015).

491 9. Pienaar, A., Bedford, R., Davis, K. & Bishop, P. N. Restoration of vision with
492 ectopic expression of human rod opsin. *Curr. Biol.* **25**, 1–35 (2015).

493 10. Lagali, P. S. *et al.* Light-activated channels targeted to ON bipolar cells restore
494 visual function in retinal degeneration. *Nat. Neurosci.* **11**, 667–675 (2008).

495 11. Lin, J. Y., Lin, M. Z., Steinbach, P. & Tsien, R. Y. Characterization of
496 Engineered Channelrhodopsin Variants with Improved Properties and Kinetics.
497 *Biophys. J.* **96**, 1803–1814 (2009).

498 12. Gossen, M. *et al.* Transcriptional activation by tetracyclines in mammalian cells.
499 *Science* **268**, 1766–9 (1995).

500 13. Tanaka, K. F. *et al.* Expanding the repertoire of optogenetically targeted cells
501 with an enhanced gene expression system. *Cell Rep.* **2**, 397–406 (2012).

502 14. Takata, N. *et al.* Optogenetic astrocyte activation evokes BOLD fMRI response
503 with oxygen consumption without neuronal activity modulation. *Glia* **66**, 2013–
504 2023 (2018).

505 15. Kanemaru, K. *et al.* In Vivo visualization of subtle, transient, and local activity of
506 astrocytes using an ultrasensitive Ca2+ indicator. *Cell Rep.* **8**, 311–318 (2014).
507 16. Rodriguez, A. R., de Sevilla Müller, L. P. & Brecha, N. C. The RNA binding
508 protein RBPMS is a selective marker of ganglion cells in the mammalian retina.
509 *J. Comp. Neurol.* **522**, 1411–43 (2014).
510 17. Tsunematsu, T. *et al.* Optogenetic manipulation of activity and temporally
511 controlled cell-specific ablation reveal a role for MCH neurons in sleep/wake
512 regulation. *J. Neurosci.* **34**, 6896–6909 (2014).
513 18. Tsubura, A., Yoshizawa, K., Kuwata, M. & Uehara, N. Animal models for
514 retinitis pigmentosa induced by MNU ; disease progression , mechanisms and
515 therapeutic trials Histology and. 933–944 (2010).
516 19. Vaney, D. I., Sivyer, B. & Taylor, W. R. Direction selectivity in the retina:
517 Symmetry and asymmetry in structure and function. *Nat. Rev. Neurosci.* **13**, 194–
518 208 (2012).
519 20. Yoshida, K. *et al.* A key role of starburst amacrine cells in originating retinal
520 directional selectivity and optokinetic eye movement. *Neuron* **30**, 771–80 (2001).
521 21. Carter-Dawson, L. D., LaVail, M. M. & Sidman, R. L. Differential effect of the
522 rd mutation on rods and cones in the mouse retina. *Invest. Ophthalmol. Vis. Sci.*

17, 489–98 (1978).

22. Association for Research in Vision and Ophthalmology., L. D., LaVail, M. M. & Sidman, R. L. *Investigative ophthalmology & visual science. Investigative Ophthalmology & Visual Science* **17**, (C.V. Mosby Co, 1977).

23. Taylor, W. R. & Smith, R. G. The role of starburst amacrine cells in visual signal processing. *Vis. Neurosci.* **29**, 73–81 (2012).

24. Yamada, E. S. *et al.* Synaptic connections of starburst amacrine cells and localization of acetylcholine receptors in primate retinas. *J. Comp. Neurol.* **461**, 76–90 (2003).

25. Yonehara, K. *et al.* Spatially asymmetric reorganization of inhibition establishes a motion-sensitive circuit. *Nature* **469**, 407–410 (2011).

26. Marc, R. E. *et al.* Heterocellular coupling between amacrine cells and ganglion cells. *Front. Neural Circuits* **12**, 1–23 (2018).

27. Völgyl, B., Chheda, S. & Bloomfield, S. A. Tracer coupling patterns of the ganglion cell subtypes in the mouse retina. *J. Comp. Neurol.* **512**, 664–687 (2009).

28. Bloomfield, S. A. & Volgyi, B. The diverse functional roles and regulation of neuronal gap junctions in the retina. *Nat Rev Neurosci* **10**, 495–506 (2009).

541 29. Sengupta, A. *et al.* Red-shifted channelrhodopsin stimulation restores light
542 responses in blind mice , macaque retina , and human retina. *EMBO Mol Med* 1–
543 17 (2016). doi:10.15252/emmm.201505699
544 30. Pan, Z. H., Ganjawala, T. H., Lu, Q., Ivanova, E. & Zhang, Z. ChR2 mutants at
545 L132 and T159 with improved operational light sensitivity for vision restoration.
546 *PLoS One* (2014). doi:10.1371/journal.pone.0098924
547 31. Wu, C., Ivanova, E., Zhang, Y. & Pan, Z.-H. rAAV-Mediated Subcellular
548 Targeting of Optogenetic Tools in Retinal Ganglion Cells In Vivo. *PLoS One* **8**,
549 e66332 (2013).
550 32. Mure, L. S. *et al.* Melanopsin-Encoded Response Properties of Intrinsically
551 Photosensitive Retinal Ganglion Cells. *Neuron* **90**, 1–12 (2016).
552 33. Keeler, A. M. & Flotte, T. R. Recombinant Adeno-Associated Virus Gene
553 Therapy in Light of Luxturna (and Zolgensma and Glybera): Where Are We, and
554 How Did We Get Here? *Annu. Rev. Virol.* **6**, 601–621 (2019).
555 34. Chaffiol, A. *et al.* A New Promoter Allows Optogenetic Vision Restoration with
556 Enhanced Sensitivity in Macaque Retina. *Mol. Ther.* **25**, 2546–2560 (2017).
557 35. Lin, B., Koizumi, A., Tanaka, N., Panda, S. & Masland, R. H. Restoration of
558 visual function in retinal degeneration mice by ectopic expression of melanopsin.

559 *Proc. Natl. Acad. Sci. U. S. A.* **105**, 16009–16014 (2008).

560 36. Strang, C. E., Renna, J. M., Amthor, F. R. & Keyser, K. T. Muscarinic
561 Acetylcholine Receptor Localization and Activation Effects on Ganglion
562 Response Properties. *Investig. Opthalmology Vis. Sci.* **51**, 2778 (2010).

563 37. Keyser, K. T. *et al.* Amacrine, ganglion, and displaced amacrine cells in the
564 rabbit retina express nicotinic acetylcholine receptors. *Vis. Neurosci.* **17**, 743–52

565 38. Dmitrieva, N. A., Strang, C. E. & Keyser, K. T. Expression of Alpha 7 Nicotinic
566 Acetylcholine Receptors by Bipolar, Amacrine, and Ganglion Cells of the Rabbit
567 Retina. *J. Histochem. Cytochem.* **55**, 461–476 (2007).

568 39. Liu, J. *et al.* Nicotinic Acetylcholine Receptor Subunits in Rhesus Monkey
569 Retina. *Investig. Opthalmology Vis. Sci.* **50**, 1408 (2009).

570 40. Blute, T. A., Strang, C., Keyser, K. T. & Eldred, W. D. Activation of the
571 cGMP/nitric oxide signal transduction system by nicotine in the retina. *Vis.*
572 *Neurosci.* **20**, 165–76

573 41. Cimini, B. A., Strang, C. E., Wotring, V. E., Keyser, K. T. & Eldred, W. D. Role
574 of acetylcholine in nitric oxide production in the salamander retina. *J. Comp.*
575 *Neurol.* **507**, 1952–1963 (2008).

576 42. Strang, C. E., Long, Y., Gavrikov, K. E., Amthor, F. R. & Keyser, K. T.

577 Nicotinic and muscarinic acetylcholine receptors shape ganglion cell response
578 properties. *J. Neurophysiol.* **113**, 203–217 (2015).
579 43. Famiglietti, E. V. J. 'Starburst' amacrine cells and cholinergic neurons: mirror-
580 symmetric on and off amacrine cells of rabbit retina. *Brain Res.* **261**, 138–144
581 (1983).
582 44. Famiglietti, E. V. Starburst amacrine cells: Morphological constancy and
583 systematic variation in the anisotropic field of rabbit retinal neurons. *J. Neurosci.*
584 **5**, 562–577 (1985).
585 45. Grailhe, R., Grabtree, G. W. & Hen, R. Human 5-HT5 receptors: the 5-HT5A
586 receptor is functional but the 5-HT5B receptor was lost during mammalian
587 evolution. *Eur. J. Pharmacol.* **418**, 157–167 (2001).
588 46. Chen, Y. *et al.* Systems pharmacology identifies drug targets for Stargardt
589 disease–associated retinal degeneration. *J. Clin. Invest.* **123**, 5119–5134 (2013).
590 47. Ikeda, H. & Wright, M. J. Receptive field organization of 'sustained' and
591 'transient' retinal ganglion cells which subserve different functional roles. *J.*
592 *Physiol.* **227**, 769–800 (1972).
593 48. Katada, Y., Kobayashi, K., Tsubota, K. & Kurihara, T. Evaluation of AAV-DJ
594 vector for retinal gene therapy. *PeerJ* (2019).

595 49. Lee, D. *et al.* Retinal dysfunction induced in a mouse model of unilateral
596 common carotid artery occlusion. *PeerJ* 1–19 (2021). doi:10.7717/peerj.11665
597 50. Kunimi, H. *et al.* Inhibition of the HIF-1α/BNIP3 pathway has a retinal
598 neuroprotective effect. *FASEB J.* **35**, 1–17 (2021).
599 51. Tabata, H., Shimizu, N., Wada, Y., Miura, K. & Kawano, K. Initiation of the
600 optokinetic response (OKR) in mice. *J. Vis.* **10**, 13–13 (2010).
601 52. Jiang, X. *et al.* A highly efficient murine model of experimental myopia. *Sci.*
602 *Rep.* **8**, 2026 (2018).
603 53. Kubota, Y., Hirashima, M., Kishi, K., Stewart, C. L. & Suda, T. Leukemia
604 inhibitory factor regulates microvessel density by modulating oxygen-dependent
605 VEGF expression in mice. *J. Clin. Invest.* **118**, 2393–403 (2008).
606 54. Kurihara, T. *et al.* Neuroprotective effects of angiotensin II type 1 receptor
607 (AT1R) blocker, telmisartan, via modulating AT1R and AT2R signaling in
608 retinal inflammation. *Invest. Ophthalmol. Vis. Sci.* **47**, 5545–52 (2006).
609
610

611 **Figures**

612 **Figure 1. Gene induction of RGCs and SACs in M4-YC and RGCs in 5B-YC**

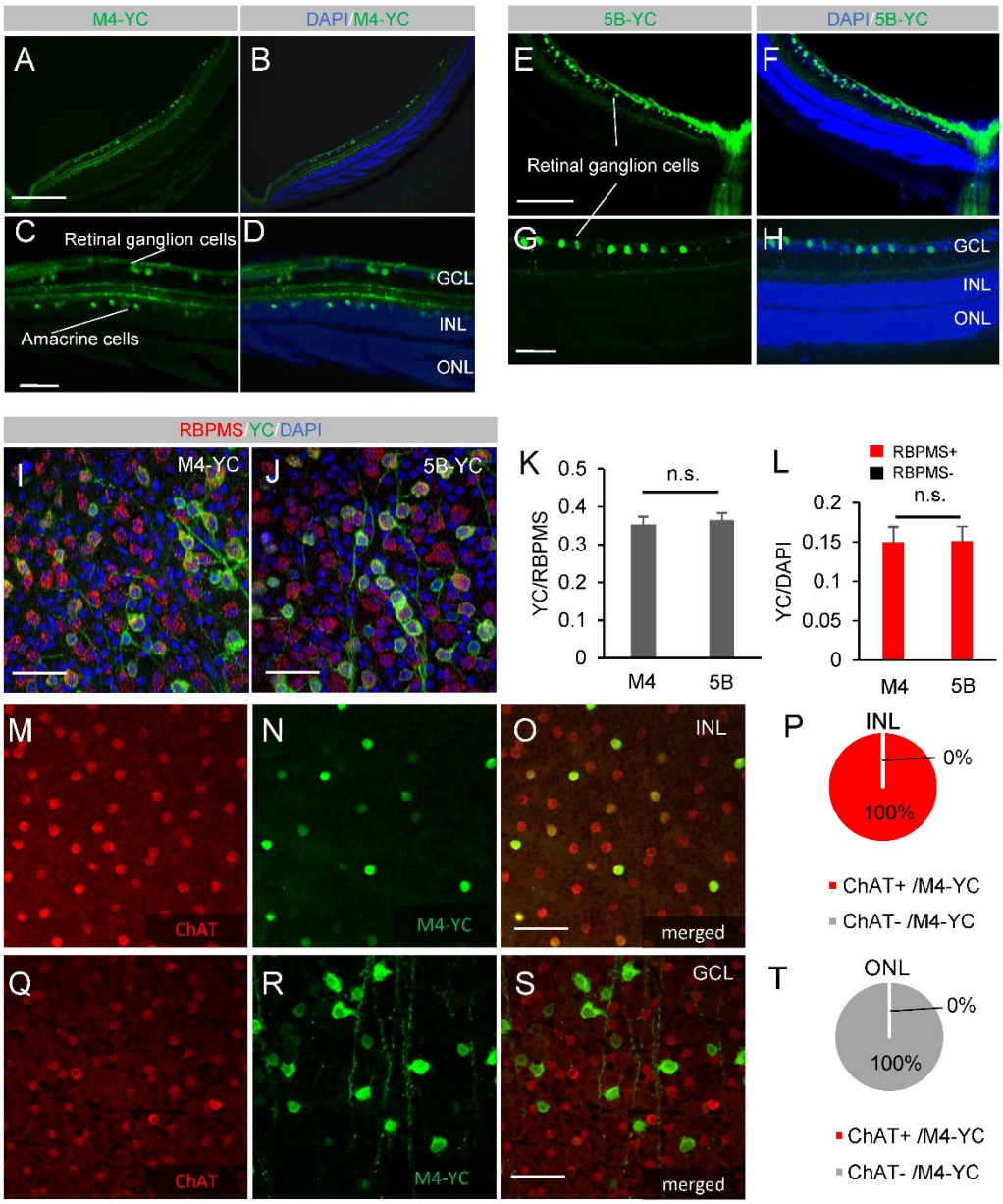

613

614 In the M4-YC mouse retina, we identified the expression of YC (green) in RGCs and
615 amacrine cells within sections (A-D). In the 5B-YC mouse retina, we identified the
616 expression of YC (green) in RGCs in sections (E-H). Coexpression of the RGC marker
617 RBPMS in flat-mounted retinas of M4-YC(I) and 5B-YC(J). Percentage of YC-positive
618 cells in RBPMS-positive (K) or DAPI-positive cells (L) and RBPMS-positive cells in YC-
619 positive cells (L) in both lines from confocal flat-mounted GCL (n = 3 retinas each). Regions
620 were chosen in each quadrant, and we obtained RBPMS, DAPI-positive, YC-positive, and
621 co-labeled cells. Coexpression of the starburst amacrine cell marker ChAT in flat-mounted
622 retinas of M4-YC in INL (M-O) and GCL (Q-S). Percentage of ChAT-positive cells in YC-
623 positive cells in M4-YC mice from INL (P) and GCL (T) (n = 3 retinas each). Error bars
624 represent the SEMs. INL, inner nuclear layer; GCL, ganglion cell layer; ONL, outer nuclear
625 layer.

626 Scale bar: 50 μm in (E). 100 μm in (B-D), (H), (I), (K), (M), (Q), and (R). 400 μm in (N).
627 500 μm in (F), (G), (O), and (P).

628

Figure 2. M4-ChR2 mouse shows a higher visual restoration effect.

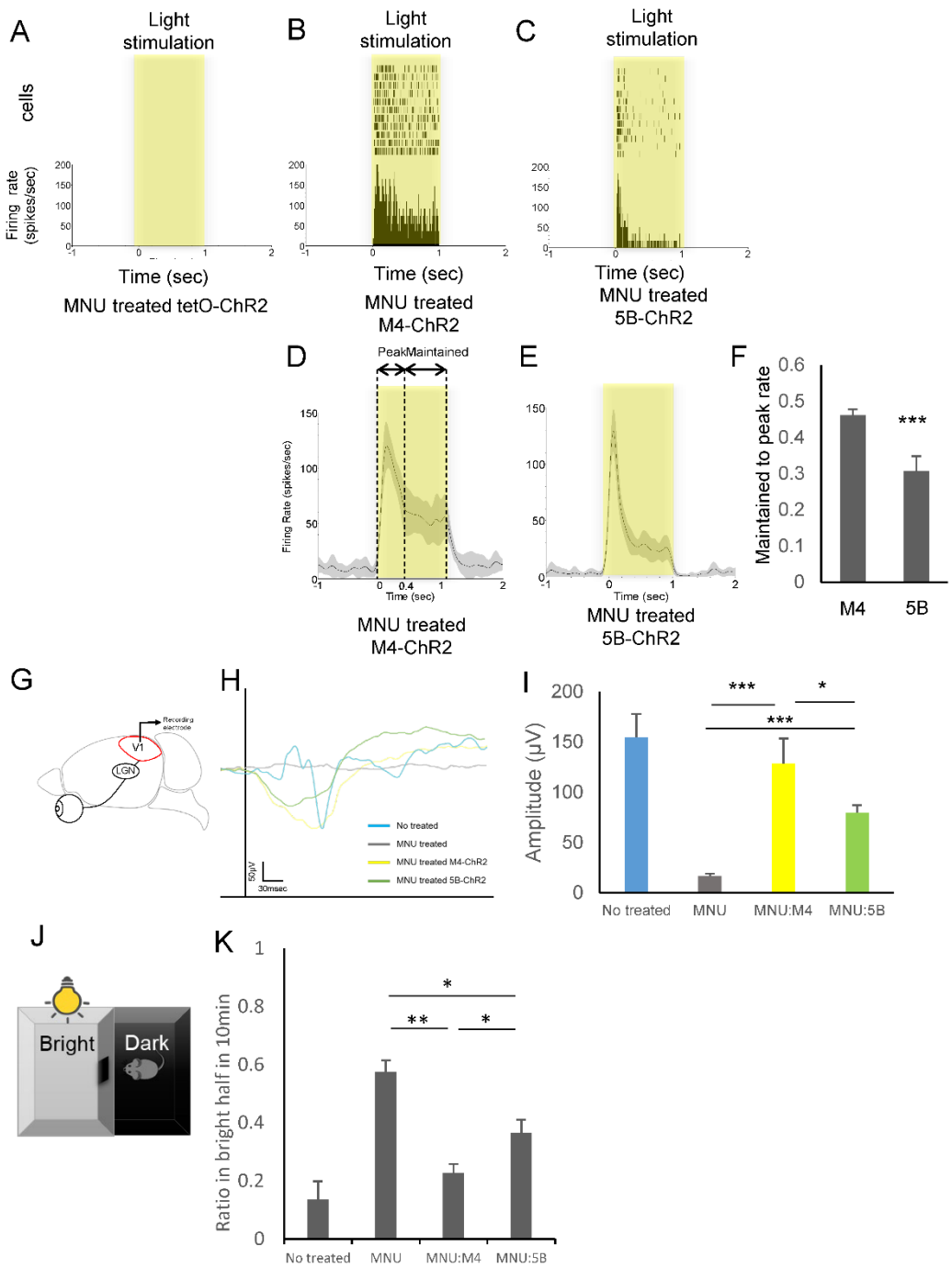

631 (A-C) Raster plots and peri-stimulus time histogram (PSTH) of light stimulation from
632 single RGCs of MNU-treated tetO-ChR, M4-ChR2, and 5B-ChR2 mice. Light intensity was
633 13.6 log photons/cm^2/s, and the duration was 1.0 seconds. (D, E) The averaged rate
634 histogram after filtering with the Gaussian function from M4-ChR2 and 5B-ChR2 mice. At
635 least 10 trials were conducted for each cell. The gray areas around the averaged traces
636 represent the SEM. (F) Maintained-to-peak ratio of the spiking responses recorded. The
637 maintained time frame is 0.4 to 1.0 seconds from light stimulation as shown in H (n = 7
638 retinas, 164 cells in MNU-treated M4-ChR2 mice, and n = 4 retinas, 127 cells in MNU-
639 treated 5B-ChR2 mice). Error bars represent SEMs. ***$p < 0.001$. Student's 2-tailed t-test.
640 (G) Schematic image of VEP measurement. (H) Representative VEP traces from MNU-
641 injected and control mice. (I) The average amplitude of the VEPs in the control tetO-ChR
642 mice (n = 4), MNU-treated tetO-ChR mice (n = 8), M4-ChR2 mice (n = 14), and 5B-ChR2
643 mice (n = 12) at 10 weeks of age. It was stimulated with a light stimulus intensity of 100-
644 ms pulses of white LED 4,000 cds/m2. Signals were low-pass filtered at 300 Hz and
645 averaged over the 60 trials. (J) Schematic image of the LDT. Mice were tested in a 30 × 45
646 × 30-cm box containing equally sized bright (200 lx at ground level) and dark chambers
647 connected by a 5 × 5-cm opening, across which the mice could move freely. Visible mice
648 feel uneasy in bright places, so staying time in the bright half gets shorter. (K) % time in

649 bright half at 10 min of control (tetO-ChR2 mice) (n = 4), MNU-injected tetO-ChR2 mice

650 (n = 8), MNU injected M4-ChR2 mice (n = 15), and MNU-injected 5B-ChR2 mice (n = 8)

651 measured from LDT. All error bars represent the SEMs. *$p < 0.05$, **$p < 0.01$, ***$p < 0.001$.

652 One-way ANOVA testing.

653 **Figure 3. Acetylcholine and gap junctions were involved in the maintained response.**

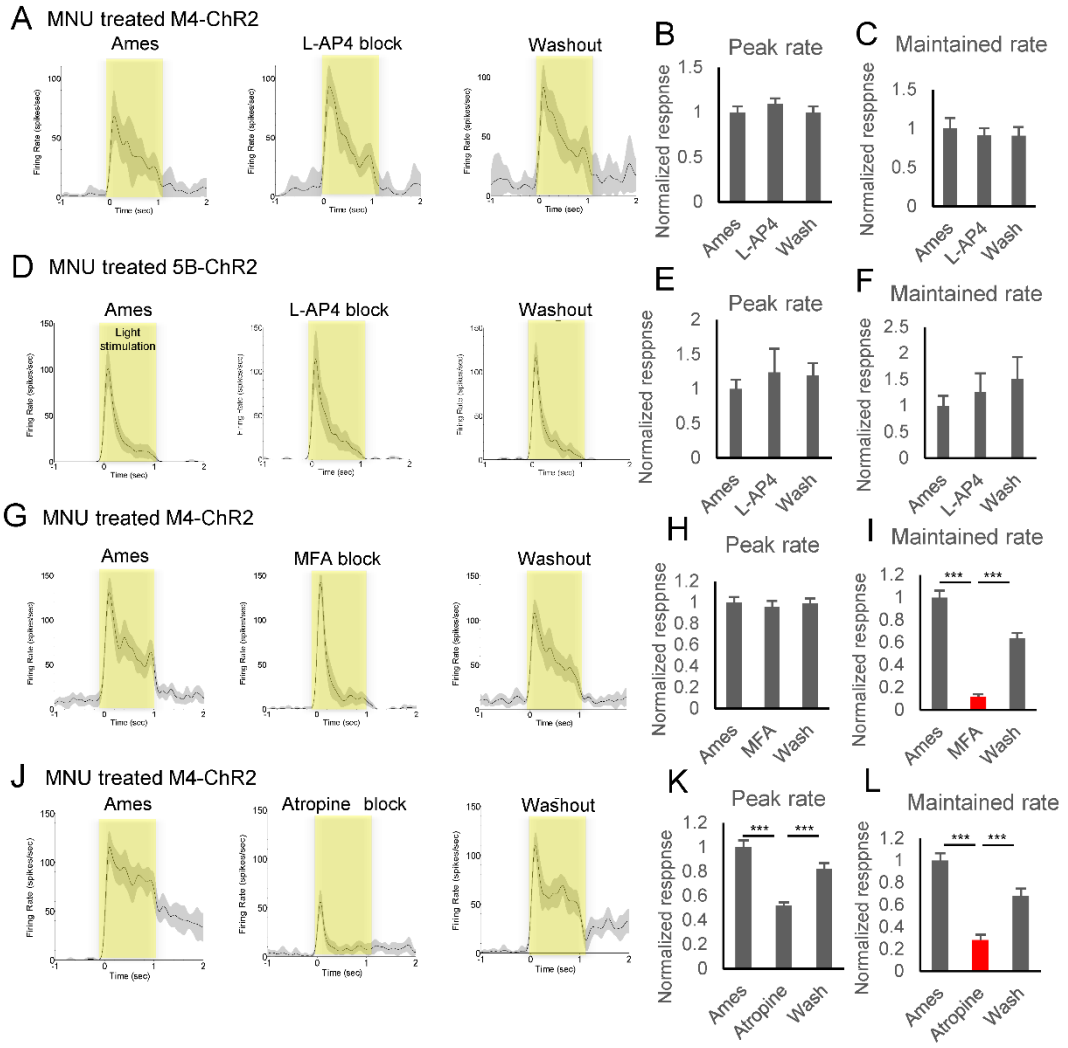

654

655 (A, D, G, J) Mean ± SEM of exemplar cell response firing rate recorded during normal

656 Ames' medium superfusion (left), in synaptic block (middle), and after washout (right).

657 MNU-treated M4-ChR2 mice with L-AP4 block (n = 3 retinas, 47 cells) (A), MNU-treated

658 5B-ChR2 mice with L-AP4 block (n = 3 retinas, 45 cells) (D), MNU-treated M4-ChR2 mice

659 with MFA block (n = 3 retinas, 85 cells) (G), MNU-treated M4-ChR2 mice with atropine

660 block (n = 3 retinas, 33 cells) (J). The gray areas around the averaged traces represent the

661 SEM. (B, C, E, F, H, I, K, L) Averaged normalized peak firing rate and maintained rate.

662 The maintained time frame is 0.4 to 1.0 seconds from light stimulation. Light intensity was

663 13.6 log photons/cm^2/s.

664 All error bars represent the SEM. ***$p < 0.001$. One-way ANOVA and Tukey's test.

665

666 **Figure 4. Induction efficiency into SACs tended to affect visual restoration.**

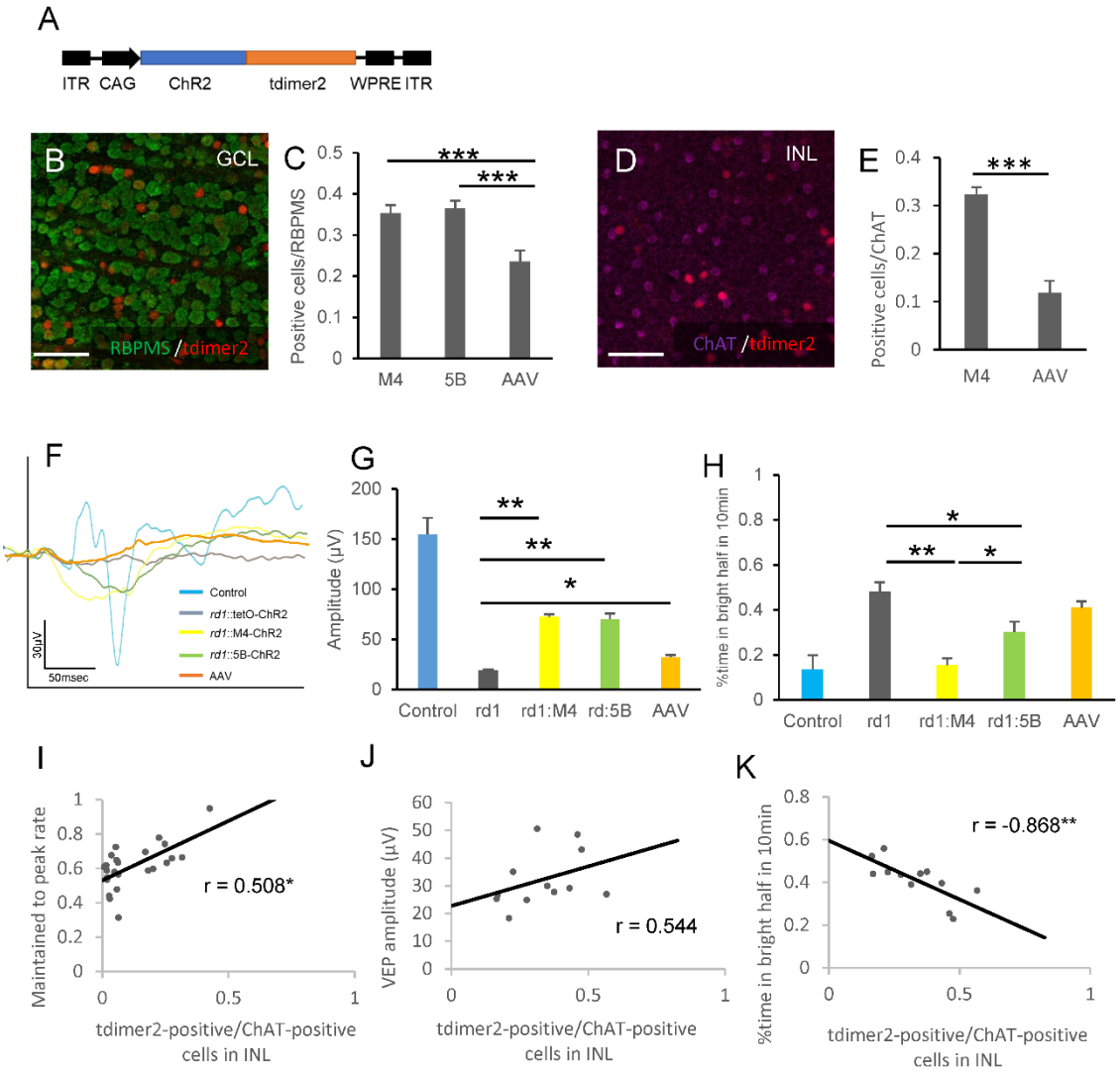

667

668 (A) The rAAV2–CAG-ChR2–tdimer2–WPRE expression cassette: ITR, inverted

669 terminal repeat; WPRE, woodchuck hepatitis virus posttranscriptional regulatory

670 element. (B-E) Coexpression of the RGC marker RBPMS (B) and starburst amacrine

671 cell marker ChAT (D) and tdimer2 in flat mounted retinas of rAAV2–CAG–tdimer2–

672 WPRE treated retinas in *rd1* mice. (C, E) Percentage of YC-positive cells in M4-YC
673 and 5B-YC mice and tdimer2-positive cells in rAAV-treated mice in RBPMS-positive
674 (C) or ChAT-positive cells (E) from confocal flat mounted retina (n = 3 retinas each).
675 Regions were chosen in each quadrant, and we obtained RBPMS, ChAT-positive,
676 YC/tdimer2-positive, and co-labeled cells. (F, G) Average VEP traces (F) and
677 quantification of its amplitudes (G) from control (tetO-ChR2) (n = 3), *rd1*::tetO-ChR2
678 (n = 6), *rd1*;M4-ChR2 (n = 12), *rd1*;5B-ChR2 (n = 12) and rAAV treated *rd1*::tetO-
679 ChR2 mice (n = 12) at 10 weeks of age. It was stimulated with 100-ms pulses of white
680 LED 4,000 cds/m^2 light stimulus intensity. Signals were low-pass filtered at 300 Hz and
681 averaged over the 60 trials. (H) % time in bright half at 10 min in control (tetO-ChR2)
682 (n = 3), *rd1*::tetO-ChR2 (n = 6), *rd1*;M4-ChR2 (n = 12), *rd1*;5B-ChR2 (n = 12) and
683 rAAV-treated *rd1*::tetO-ChR2 mice (n = 12) measured from LDT. (I-K) Correlation
684 between transfection efficiency into SACs (tdimer2-positive cells/ChAT-positive cells
685 in INL) and maintained to peak rate (I) (n = 24), VEP amplitude (J) (n = 24) and % time
686 in bright half in LDT (K) (n = 12).

687 All error bars represent the SEMs. INL, inner nuclear layer; GCL, ganglion cell layer.
688 Scale bars, 50 μm in (B), (D), n.s.: not significant, *p < 0.05, **p < 0.01, ***p < 0.001.
689 unpaired t-test (E),Games-Howell test (C, G, H), Pearson's correlation coefficient (I-K).